Magnetic iron oxide and the effect of grafting on the magnetic properties

L. Truong Phuoc J. Jouhannaud and G. Pourroy
Institut de Physique et Chimie des Matériaux de Strasbourg IPCMS, UMR 7504 CNRS-Université de Strasbourg-ECPM, 23 rue du Loess BP 43, 67034 Strasbourg cedex 2, France

ABSTRACT

In our studies, related to projects developing nanoparticles for sentinel node detection of breast cancer [Nanomagdye FP7, EU project grant agreement nr NMP3-SL-2008-214032 and Nanomatrix INTERREG IV program Upper Rhine Valley A21], we focused on the magnetic iron oxide nanoparticles in 10-40 nm range made by precipitation in aqueous media, on the functionalization by dendrons ensuring the stabilization in aqueous media and on the effect of grafting on the magnetic properties. By combining magnetic measurements, X-ray diffraction and Mössbauer spectrometry, we showed that the nanoparticles can be described by a core-shell model, that is, a magnetite core surrounded by an oxidized layer close to maghemite. The fractional volume of maghemite increases as the particle size decreases so that below 20 nm, the particle is oxidized in the whole volume and the nanoparticles cannot be properly labeled as "magnetite". The oxide/molecule interactions have a strong effect on the magnetic structure and properties. In case of phosphonate coupling agent, the saturation magnetization is increased and no spin canting is observed due to a covalent bonding.

Keywords: iron oxide nanoparticle, magnetic structure, size, grafting, dendrons

1. INTRODUCTION

The detection of diseases at an early stage is significant for improving the prognosis and the treatments efficiency. Indeed, faster the disease is detected, more efficient is the treatment and better the prognosis. Many imaging techniques are currently available for visualizing the body and detecting anomalies, such as magnetic resonance imaging (MRI), positron emission tomography (PET), single-photon emission tomography (SPECT), X-rays and ultrasonography (US). However, the image resolution depends on the technique and combining probes increase the success rates. In cancer surgery, imaging the lymph circuit is a key point for the surgeons to estimate the grade of the tumor and anticipate the prognosis [1]. Indeed, if the sentinel lymph node (SLN), i.e. the first node draining the primary tumor, contains metastatic cancer cells, a more aggressive surgery is required in order to remove all the lymph basin. The methods generally used are based on radiocolloids labelled with ^{99m}Tc and/or on vital blue dyes injected in the peritumoral region [2-4]. The radiocolloid is injected several hours before surgery and detected by means of a gamma probe during surgery. The dye circulates rapidly in the lymph circuit and is visually detected by the surgeon. Nevertheless, both methods suffer from drawbacks: for the former, a low spatial resolution and an exposure to ionizing radiations combined with the need of adapted technical environments, and for the latter, a persistent skin stain in some cases despite a more specific localization. Furthermore, the success rate is increased when the two methods are used jointly. In this context, the development of magnetic markers to be used alone or combined with an optical marker in multimodal nanoparticles appears to be an interesting alternative, as recent progress have been done in optical and magnetic probes sensitivities [5-10].

> We present results, related to projects developing nanoparticles for sentinel node detection of breast cancer [Nanomagdye FP7, EU project grant agreement nr NMP3-SL-2008-214032 and Nanomatrix INTERREG IV program Upper Rhine Valley A21]. Our strategy was to design magnetic-optic nanomarkers. We synthesized dendronized iron oxide nanoparticles as schematized in

Figure 1, to be detected during surgery by magnetic and/or optical hand-held probes [11-12]. Magnetite (Fe_3O_4) and maghemite (γ-Fe_2O_3) are the most used magnetic iron oxides because of their low cost and biocompatibility. Both crystallize in the spinel structure (spatial group Fd-3m). They can be distinguished by their lattice parameter a = 0. 8396 nm (JCPDS No. 19-0629) for magnetite and 0.8346 nm for maghemite (JCPDS file 39-1346). Furthermore, magnetite undergoes a crystallographic transition at 120K called Verwey transition, also visible on the thermal evolution of the

Nanosystems in Engineering and Medicine, edited by Sang H. Choi, Jin-Ho Choy, Uhn Lee, Vijay K. Varadan,
Proc. of SPIE Vol. 8548, 85480M · © 2012 SPIE · CCC code: 1605-742/12/$18 · doi: 10.1117/12.999989

magnetization [13]. Two main methods have been developed to obtain magnetite nanoparticles: the decomposition of organometallic precursors such as iron pentacarbonyl, iron(III) cupferronate ($FeCup_3$) or iron (III) acetylacetonate ($Fe(acac)_3$), in the presence of surfactants and the precipitation of Fe^{2+} and Fe^{3+} ions into a basic aqueous media [14-17]. Most of nanoparticles have sizes around or lower than 10 nm and exhibit a superparamagnetic behaviour usable in MRI applications [18]. The recent development of magnetic particle imaging or hand-held probes for sentinel node detection in cancer surgery requires particles of size close to the blocked monodomain i.e. in the 15-30 nm size range [19-22]. Therefore, the elaboration of such particles suspensions becomes of the utmost importance. Our strategy was based 1) on the elaboration of magnetic iron oxides with controlled sizes, high susceptibility and magnetization; 2) on the grafting of dendritic molecules; they are discrete and monodisperse entities which relevant characteristics (size, hydrophilicity, molecular weight…) can be tuned as a function of their generation. They are already used in nuclear medical imaging [21-22] 3) on phosphonates as coupling agent justified by previous studies that have evidenced that they allow a significantly higher grafting rate and a stronger binding than carboxylate anchors [23-25].

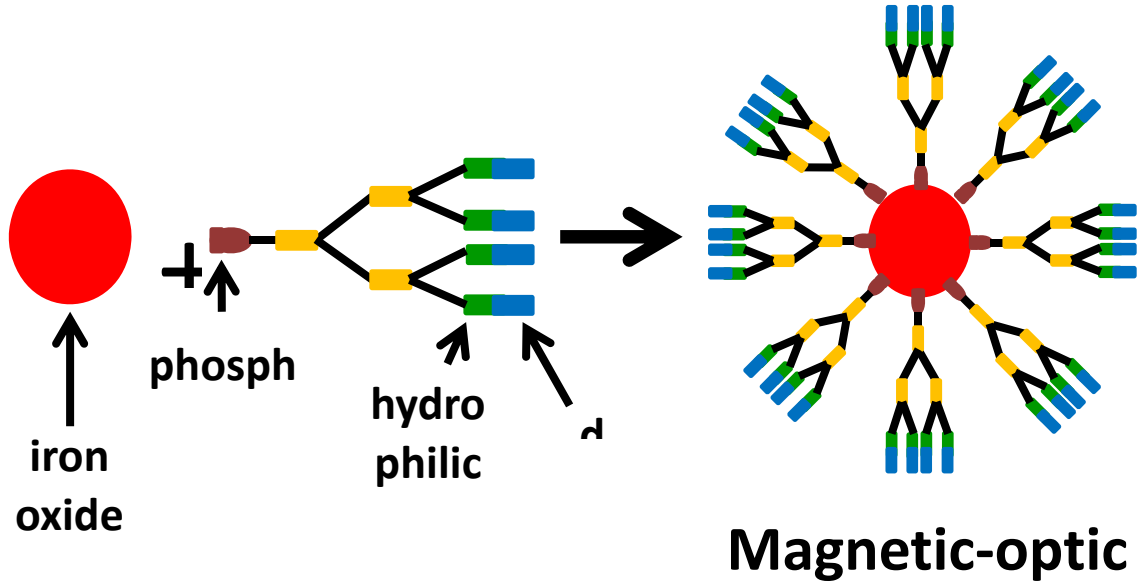

Figure 1. Schematic view of the multifunctional dendronized iron oxide.

We present here a review on the elaboration and the physical properties of iron oxide obtained by coprecipitation in water, the grafting of dendrons and the physical properties of the markers [26-29]. The precipitation method allows us to obtain great quantities of iron oxide in one batch in water with high magnetizations compared to the organic precursors method. We focus particularly on improving the size and the size distribution as it is a key point for getting the required magnetic properties, on the structure of the oxide according to the size in terms of magnetite and maghemite and on the effect of the grafting on the magnetic properties and structure of the oxide.

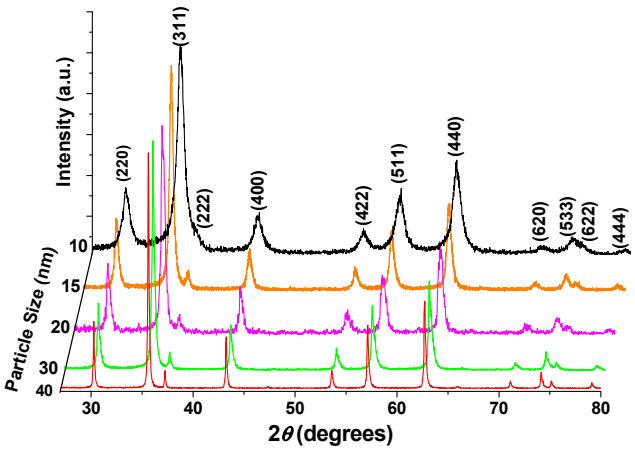

Figure 2. X-ray diffraction patterns of magnetic iron oxide for five different sizes, 10, 15, 20, 30 and 40 nm. The diffraction lines are labeled by hkl Miller indices in the spinel structure.

2. IRON OXIDE NANOPARTICLES

The nanoparticles (NPs) were prepared by precipitation of ferrous Fe^{2+} and ferric Fe^{3+} ions in water followed by a hydrothermal treatment between 200 and 250°C [27,29]. Ferrous to ferric iron ratio was taken in 1:2 ratio in order to obtain magnetite according to the reaction:

$$Fe^{2+} + 2Fe^{3+} + 8OH^- \rightarrow Fe_3O_4 + 8H_2O \quad (1)$$

Ammonium bases, tetramethyl-, tetraethyl- or tetrapropyl ammonium hydroxide, were added to the iron chloride solutions, so that the pH increased during the reaction. In the great majority of previously published results on iron oxides synthesized by precipitation, the two cations are precipitated simultaneously by adding the chlorides to the base, so that the pH is basic throughout the reaction [30]. In our case, FeOOH precipitates first around pH=2.75-3. At approximately pH 5-6, Fe^{2+} precipitates. According to previous studies, Fe^{2+} adsorbs at the ferric hydroxide surface. Increasing the pH gives rise to dehydration of hydroxides and leads to the formation of magnetite facilitated by electron hoping between Fe^{2+} and Fe^{3+}. When pH 11 is reached, a magnetic black powder precipitates. The whole sample is then submitted to the hydrothermal treatment.

The crystallographic structure was checked by powder X-ray diffraction (XRD) using a Bruker D8 Advance diffractometer equipped with a quartz monochromator, a Sol-X energy dispersive X-ray detector and Cu Kα radiation (λ = 0.154059 nm). All the peaks were indexed in the spinel structure (spatial group Fd-3m, (277), JCPDS No. 19-0629) (Figure 2). Neither hematite (α-Fe_2O_3) nor partially ordered maghemite were observed in the pattern. The lattice parameters were close to the magnetite one (a = 0. 8396 nm) and far from the maghemite one (0.8346 nm, JCPDS file 39-1346) showing that magnetite is partially oxidized when put in contact with air. Oxidation of Fe^{2+} to Fe^{3+} leads to a cation-deficient spinel, and the composition ranges from magnetite (x = 0) to maghemite (x = 1/3) according to the formula: $[Fe^{3+}]_A\,[Fe^{2+}{}_{1-3x}\,Fe^{3+}{}_{1+2x}\,\square_x\,]_B\,O_4$ in which □ represents vacancies.

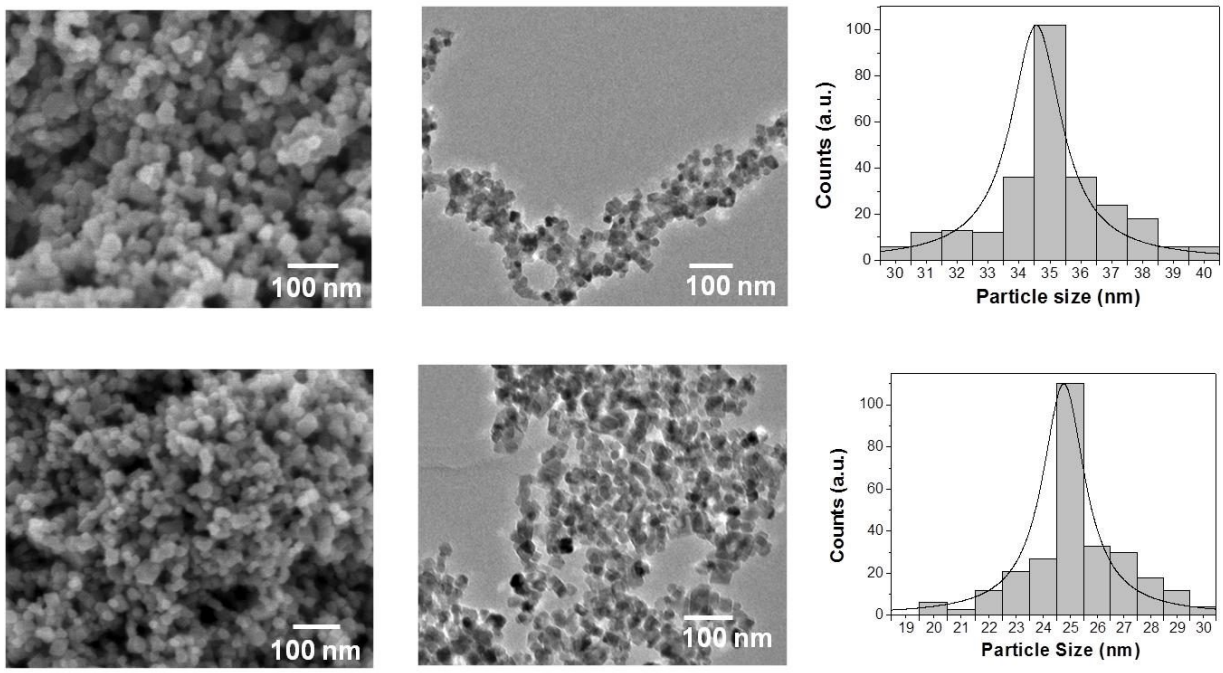

Figure 3. Typical scanning electron microscopy (left) and transmission electron microscopy (middle) images of magnetic iron oxide. Size distribution determined by using ImageJ software (left).

The nanoparticles were observed by scanning electron microscopy (SEM) (Figure 3-left). The particle size was determined using three methods:

- X-ray diffraction: the peak width gives the diffracting volume diameter D according to the Debye-Scherrer equation, $\Delta(2\theta) = 0.9\lambda / D\cos(\theta_0)$.
- Specific area measurements determined by BET method. The experimental value S is related to the particle diameter ϕ according to $\phi(nm) = 6000/\mu S$ where μ is the density
- Particles imaging by transmission electron microscopy (Figure 3-middle) and determination of particle sizes using ImageJ software (Figure 3-right). The counting was performed on 150 to 200 particles for each sample.

The three methods gave the same values showing that the diffracting volume was extended on the whole particle and consequently that the particles are not polycristalline. The diameters ranged from 40 and 22 nm for $N(CH_3)_4OH$, 35 and 10 nm for $N(C_2H_5)_4OH$ and 25 and 12 nm for $N(C_3H_7)_4OH$ (Figure 3). We showed that 1) for identical quantities of base, the particle sizes decrease as the length of the alkyl group of the ammonium base increases; 2) for each base, when the quantity of added base (i.e. pH) increases, the size also decreases.

The composition of nanoparticles in terms of maghemite to magnetite ratio was determined by combining Mössbauer spectrometry and magnetic measurements [27,29]. The Mössbauer spectra are given in [29]. The spectra recorded on larger particles (> 20 nm) at 300 K are similar to those usually observed for magnetite. When the size is lower than 20 nm, the magnetic hyperfine structure is not resolved, consisting of broadened, overlapped and asymmetrical lines originating from the occurrence of superparamagnetic relaxation phenomena. The mean stoichiometry was estimated from the mean isomer shift. The global formula was written as $Fe_{3-x}O_4$. The thermal evolution of magnetization points out the Verwey transition around 120K for nanoparticles larger than 20 nm (Figure 4). Therefore, above 20 nm, the nanoparticles are made of a magnetite core surrounded by an oxidized shell close to maghemite. The Verwey transition temperature decreases for the 25 and 20 nm nanoparticles, probably because the magnetite core size decreases. Below 20 nm, the nanoparticles are oxidized in the whole volume and the Verwey transition disappears.

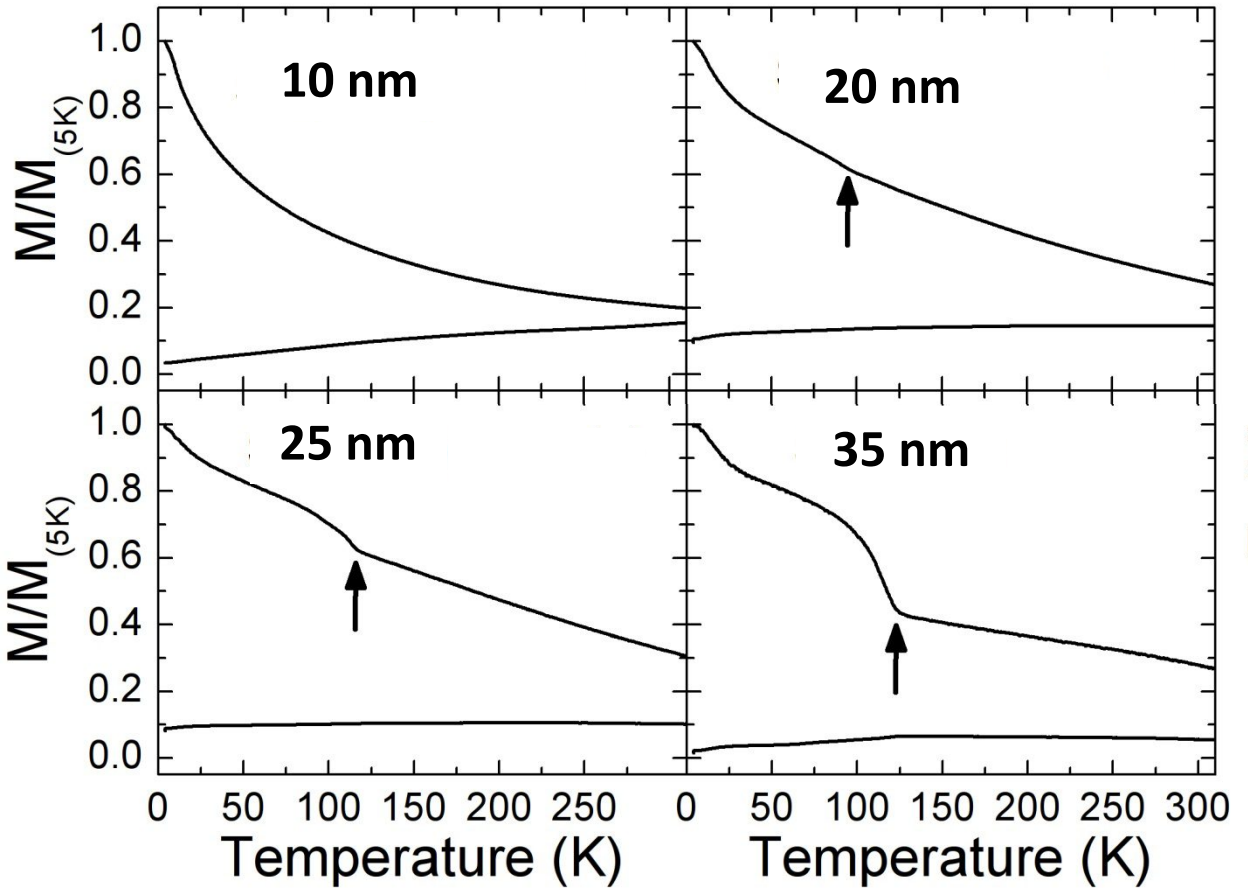

Figure 4. ZFC/FC plots for magnetite nanoparticles of average size: 10nm, 20nm, 25nm and 35nm [ ]. M5K corresponds to the magnetization under FC condition at 5K [29].

3. WATER SOLUBLE DENDRONIZED IRON OXIDE

For biomedical applications, iron oxide nanoparticles have to be stabilized in aqueous suspensions. Numerous strategies have been developed to ensure suspension stability and/or bringing a suitable biocompatible coating. To this end, we chose to graft dendrons, schematized in Figures 1 and 5, onto the oxide surface [11,22]. The dendrons are characterized by a phosphonate anchor and polyethyleneglycol chains. Additional groups, such as dyes, could be attached at the periphery. The grafting of dendrons onto the oxide surface was done in water at various pH. Typical conditions are as follow: 50 mg of nanoparticles dispersed in 25 ml degassed water, were sonicated for 10 min. A given amount of dendritic triethyleneglycol phosphonate was dissolved in 12.5mL degassed water. The reaction mixture was submitted to ultrasound for 90 min at 37°C and washed by ultrafiltration.

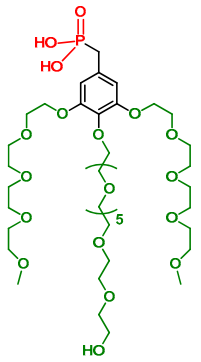

D3

Figure 5.Scheme of the dendron [22].

The grafting mechanism was investigated on 9 nm and 39 nm nanoparticles [28]. The molecules grafting was confirmed by thermogravimetric (TG) and differential thermal (TD) analyses in air. The dendron decomposes in air and the resulting weight corresponds to the phosphate part. A weight loss is observed on the TG curve of dendronized iron oxide, but due to the oxidation of magnetite core in air, the precise amount of molecules cannot be determined. A more precise determination was undertaken by UV-Visible spectroscopy and chemical analysis. The powders were separated from the liquid and freeze-dried to be characterized. The grafting rate was studied either directly by performing chemical analysis on the dendronized NPs by Inductively Coupled Plasma / Atomic Emission Spectroscopy (ICP-AES), or undirectly through UV-visible analyses of the washing solutions. Indeed, UV-visible spectra of the dendron exhibited an absorption band at 270 nm due to the aromatic ring.

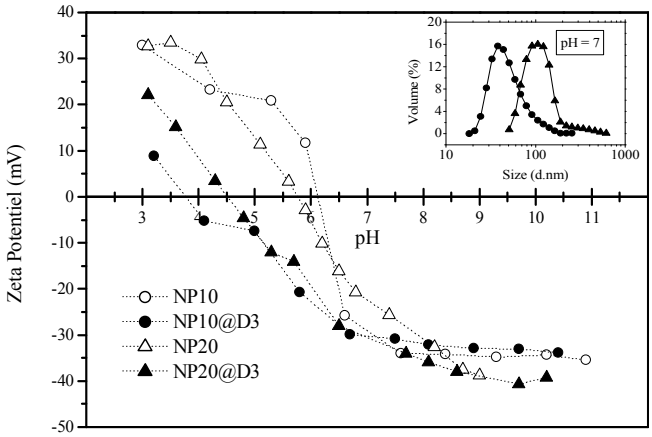

Figure 6. Zeta potential of bare 10 nm (NP10) and 20 nm (NP20) nanoparticles and the corresponding D3 dendronized NPs. The inset displays the hydrodynamic diameters of aqueous suspensions of dendronized NPs at pH7.

In order to study the parameters controlling the grafting, various amounts of dendrons have been added to the aqueous suspension of nanoparticles[28]. Only a part of dendrons binds to the oxide nanoparticles. The grafting occurs by interaction of negatively charged phosphate groups with both positively charged groups and hydroxyl sites at the surface of magnetite [26]. The variation of Zeta potentials versus pH depicts the charge at the surface of nanoparticles (Figure 6). The isoelectric points (IEP), defined as the pH at which the zeta potential value is zero, are located at pH=6 for bare nanoparticles. Between 2.7 and 6, the surface of magnetite is therefore always positively charged and the grafting occurs

in this pH range. For increasing amounts of molecules in solution, the pH decreases due to the acidic character of the phosphonate. But, simultaneously, the amounts of negatively charged molecules decrease. Indeed, as the molecule amounts go on increasing, the pH reaches the pKa value of the dendron molecules for which the molecules bear no more charges and the electrostatic force disappears as well. Therefore, the grafting rate decreases, confirming thus the relevance of electrostatic interactions in the grafting of molecules through a phosphonate group in water. The zeta potential curves of grafted nanoparticles as a function of pH are shifted towards lower pH values (Figure 6). In the two cases, the isoelectric points are between 4 and 4.5, and the zeta potential values at pH = 7 are around -30 mV for both pegylated nanoparticles. This value is higher than that reported for nanoparticles pegylated by other methods. That demonstrates the great interest in grafting dendron molecules using a phosphonate group as coupling agent in order to stabilize iron oxide suspensions by electrostatic repulsions in physiological media. Moreover, the three neutral PEG chains at the end of the molecule provide an additional steric repulsion improving the suspension stability. The mean hydrodynamic diameters $D_V(50)$ determined by Diffusion Light Scattering (DLS)were equal to 45 nm for NP10@**D3** and 100 nm for NP20@**D3** (Figure 6 inset).

4. EFFECT OF GRAFTING ON THE MAGNETIC PROPERTIES

Regarding the magnetic properties, the magnetization values of grafted nanoparticles are slightly decreased for the smallest nanoparticles and kept constant for the biggest nanoparticles (Figure 7-left). The hysteresis cycles recorded on grafted 9 nm and 39 nm nanoparticles show that (1) the superparamagnetic behaviour of the former has been preserved as no coercive field is observed and the saturation magnetization has slightly decreased from 57(1) emu/g up to 55(1) emu/g; (2) the 39 nm saturation magnetization equal to 81(1) emu/g was not changed after grafting (Figure 7-right). However, due to the organic molecule amount (85mg/g and 39 mg/g respectively), the expected saturation magnetization would be decreased up to 52 emu/g and 79 emu/g respectively. That means that the saturation magnetization of the iron oxide itself was increased up to 60(1) and 83(1) emu/g for 9 nm and 39 nm nanoparticles respectively. That has been explained by investigating the magnetic structure of the oxide by Mössbauer spectroscopy[24]. The phosphonate entity which bounds the molecule to the surface modifies the magnetic structure of the oxidized surface layer. The maghemite layer of non-grafted iron oxides has a canted magnetic structure. In grafted iron oxide, the canting has disappeared due to super-super exchange interactions between the iron atoms through the phosphonate. That leads to an increase of the magnetization in the surface layer, which compensates the decrease of magnetization due to the organic layer.

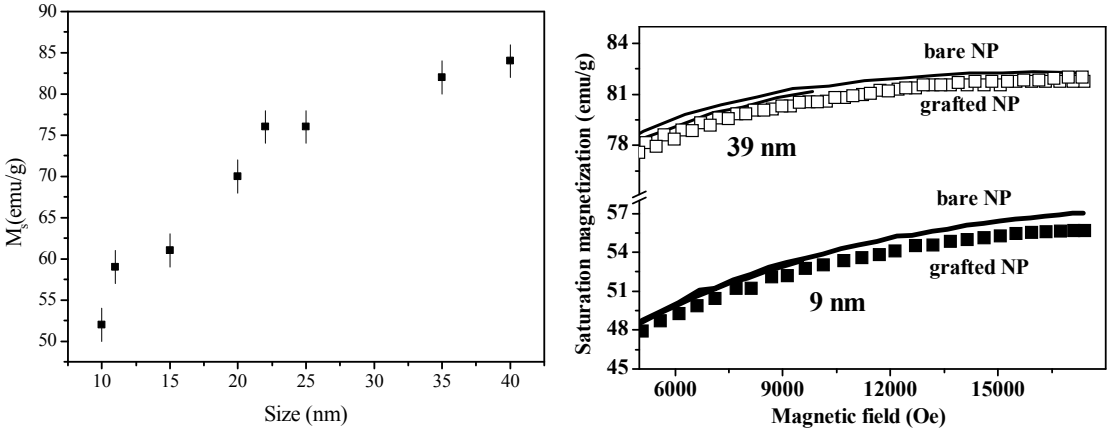

Figure 7: Variation of saturation magnetization versus the nanoparticle size (left) and saturation magnetization of bare and grafted 9nm and 39 nm nanoparticles (right).

5. CONCLUSION

The elaboration of magnetic markers for biomedical applications is a hot topic. The control of the composition and the size, as well as the knowledge of the interactions between the oxide and the organic shell, are of significant importance to predict the magnetic behavior, and therefore for applications.

ACKNOWLEDGMENTS

The research leading to these results has received funding from the European Community's Seventh Framework Programme (FP7 2007-2013) under grant agreement nr NMP3-SL-2008-214032 NANOMAGDYE and from INTERREG IV Upper Rhine Valley (A21-NANOMATRIX).

REFERENCES

[1] Koopsa, H. S., Dotinga, M. H. E., De Vriesa, J., Tieboschb, A. T. M. G., Plukkera, J. Th., Hoekstraa, H. J. and Piers, D. A., "Sentinel node biopsy as a surgical staging method for solid cancers," Radiotherapy and Oncology 51, 1-7 (1999).

[2] Ravizzini, G., Turkbey, B., Barett, T., Kobayashi, H. and Choyke, P. L., "Nanoparticles in sentinel lymph node mapping," Wires: Nanomedicine and Nanobiotechnology 1, 610-623 (2009).

[3] Jain, R., Dandekar, P., Patravale, V., "Diagnostic nanocarriers for sentinel lymph node imaging," Journal of Controlled Release 138, 90-102 (2009).

[4] Schrenk, P., Hochreiner, G., Fridrik, M. and Wayand, W., "Sentinel node biopsy performed before preoperative chemotherapy for axillary lymph node staging in breast cancer," The breast journal 9, 282-287 (2003).

[5] Malvindi, M. A., Greco, A., Conversano, F., Figuerola, A., Corti, M., Bonora, M., Lascialfari, A., Doumari, H. A., Moscardini, M., Cingolani, R., Gigli, G., Casciaro, S., Pellegrino, T. and Ragusa, A., "Magnetic/Silica Nanocomposites as Dual-Mode Contrast Agents for Combined Magnetic Resonance Imaging and Ultrasonography," Adv. Funct. Mater. 21, 2548–2555 (2011).

[6] Corato, R. Di, Bigall, N. C., Ragusa, A., Dorfs, D., Genovese, A., Marotta, R., Manna, L. and Pellegrino, T., "Multifunctional Nanobeads Based on Quantum Dots and Magnetic Nanoparticles," Synthesis and Cancer Cell Targeting and Sorting, ACSnano 5, 1109–1121 (2011).

[7] Tellier, F., Ravelo, R., Simon, H., Chabrier, R., Steibel, J. and Poulet, P., "Sentinel lymph node detection by an optical method using scattered photons," Biomedical Optics Express 1, 902-910 (2010).

[8] Vértesy, G., Gasparics, A. and Szöllősy, J., "High sensitivity magnetic field sensor," Sensors and Actuators A: physical 85, 202-208 (2000).

[9] Miyashiro, I., Kishi, K., Yano, M., Tanaka, K., Motoori, M., Ohue, M., et al., "Laparoscopic detection of sentinel node in gastric cancer surgery by indocyanine green fluorescence imaging," Surgical Endoscopy 25, 1672-1676 (2011).

[10] Hattersley, S. R. and Pankhurst, Q. A., "Hand-held magnetic probe apparatus for locating magnetic nanoparticle marker in sentinel node," PCT Int. Appl. (2011).

[11] Lamanna, G., Kueny-Stotz, M., Mamlouk-Chaouachi, H., Ghobril, C., Basly, B., Bertin, A., Miladi, I., Billotey, C., Pourroy, G., Begin-Colin, S. and Felder-Flesch, D., "Dendronized iron oxide nanoparticles for multimodal imaging," Biomaterials 32(33), 8562-8573 (2011).

[12] Basly B., Felder-Flesch D., Perriat P., Billotey C., Taleb J., Pourroy G. and Begin-Colin S. "Dendronized iron oxide nanoparticles as contrast agent for MRI" Chem. Comm. 46(6), 985-987, (2010)

[13] Aragon, R., Shepherd, J. P., Koenitzer, J. W., Buttrey, D. J., Rasmussen, R. J. and Honig, J. M., "Influence of non-stoechiometry on the Verwey transition in $Fe_{(3-\delta)}O_4$," J. Appl. Phys. 57, 3221-3222 (1985).

[14] Hyeon, T., Lee, S. S., Park, J., Chung, Y. and Na, H. B., "Synthesis of Highly Crystalline and Monodisperse Maghemite Nanocrystallites without a Size-Selection Process," J. Am. Chem. Soc. 123, 12798-12801 (2001).

[15] Rockenberger, J., Scher, E. C. and Alivisatos, A. P., "A New Nonhydrolytic Single-Precursor Approach to Surfactant-Capped Nanocrystals of Transition Metal Oxides," J. Am. Chem. Soc. 121, 11595 (1999).

[16] Sun, S., Zeng, H., Robinson, D. B., Raoux, S., Rice, P. M., Wang, S. X. and Li, G., "Monodisperse MFe2O4 (M = Fe, Co, Mn) Nanoparticles," J. Am. Chem. Soc. 126, 273 (2004).

[17] Lu, A.-H., Salabas, E. L. and Schüth, F., "Magnetic nanoparticles: synthesis, protection, functionalization, and application," Angew. Chem. Int. Ed. 46, 1222-1244 (2007).

[18] Laurent, S., Forge, D., Port, M., Roch, A., Robic, C., Vander Elst, L. and Muller, R. N., "Magnetic Iron Oxide Nanoparticles: Synthesis, Stabilization, Vectorization, Physicochemical Characterizations, and Biological Applications," Chem. Rev. 108, 2064–2110 (2008).

[19] Ferguson, R. M., Khandhar, A. P. and Krishnan, K. M., "Tracer design for magnetic particle imaging," J Appl. Phys. 111 (2012).

[20] Goodwill, P. W., Saritas, E. U., Croft, L. R., Kim, T. N., Krishnan, K. M., Schaffer, D. V. and Conolly, S. M., "X-Space MPI: Magnetic Nanoparticles for Safe Medical Imaging" Advanced materials 24(28), 3870–3877, (2012).
[21] Ghobril, C., Lamanna, G., Kueny-Stotz, M., Garofalo, A.; Billotey, C. and Felder-Flesch, D., "Dendrimers in nuclear medical imaging," New Journal of Chemistry, 36(2), 310-323 (2012).
[22] Kueny-Stotz, M., Mamlouk-Chaouachi, H. and Felder-Flesch, D., "Synthesis of Patent Blue derivatized hydrophilic dendrons dedicated to sentinel node detection in breast cancer," Tetrahedron Lett 52, 2906 (2011).
[23] Boyer, C., Bulmus, V., Priyanto, P., Teoh, W. Y., Amal, R. and Davis, T. P., "The stabilization and bio-functionalization of iron oxide nanoparticles using heterotelechelic polymers," J. Mater. Chem. 19, 111-123 (2009).
[24] Daou, T. J., Buathong, S., Ung, D., Donnio, B., Pourroy, G., Guillon, D. and Bégin, S., "Investigation of the grafting rate of organic molecules on the surface of magnetite nanoparticles as a function of the coupling agent," Sensors and Actuators B 126, 159-162 (2007).
[25] Daou, T. J., Greneche, J. M., Pourroy, G., Buathong, S., Derory, A., Ulhaq-Bouillet, C., Donnio, B., Guillon, D. and Bégin-Colin, S., "Coupling Agent Effect on Magnetic Properties of Functionalized Magnetite-Based Nanoparticles," Chem. Mater. 20, 5869-5875 (2008).
[26] Daou, T. J., Bégin-Colin, S., Greneche, J. M., Thomas, F., Derory, A., Bernhardt, P., Legare, P. and Pourroy, G., "Phosphate Adsorption Properties of Magnetite-Based Nanoparticles," Chemistry of Materials 19(18), 4494-4505 (2007).
[27] Daou, T. J., Pourroy, G., Bégin-Colin, S., Greneche, J. M., Ulhaq-Bouillet, C., Legare, P., Bernhardt, P., Leuvrey, C. and Rogez, G., "Hydrothermal Synthesis of Monodisperse Magnetite Nanoparticles," Chemistry of Materials 18(18), 4399-4404 (2006).
[28] Daou, T. J., Pourroy, G., Greneche, J. M., Bertin, A., Felder-Flesch, D. and Bégin-Colin, S., "Water soluble dendronized iron oxide nanoparticles," Dalton Trans., 4442-4449 (2009).
[29] Santoyo Salazar, J., Perez, L., De Abril, O., Truong Phuoc, L., Ihiawakrim, D., Vazquez, M., Greneche, J.-M., Bégin-Colin, S. and Pourroy, G., "Magnetic Iron oxide nanoparticles in 10-40 nm range: composition in terms of magnetite/maghemite ratio, and effect on the magnetic properties," Chem. Mater. 23(6), 1379-1386 (2011).
[30] Vayssieres, L., Chaneac, C., Tronc, E. and Jolivet, J. P., "Size Tailoring of Magnetite Particles Formed by Aqueous Precipitation: An Example of Thermodynamic Stability of Nanometric Oxide Particles," Journal of colloid and interface science 205, 205–212 (1998).
[31] Viart, N., Pourroy, G. and Greneche, J.-M., "Study of metal-ferrite composites: Complementary use of ^{57}Fe Mossbauer spectrometry, x-ray diffraction and TG analysis," European Physical Journal: Applied Physics 18(1), 33-40 (2002).